communications materials

Article

https://doi.org/10.1038/s43246-024-00476-6

Directly visualizing individual polyorganophosphazenes and their single-chain complexes with proteins

Raman Hlushko [1], Edwin Pozharski [1], Vivek M. Prabhu [2] & Alexander K. Andrianov [1]

Polyorganophosphazenes are water-soluble macromolecules with immunoadjuvant activity that self-assemble with proteins to enable biological functionality. Direct imaging by cryogenic electron microscopy uncovers the coil structure of those highly charged macromolecules. Here, we successfully visualize individual polymer chains within the vitrified state in the absence of additives for contrast enhancement which is attributed to the high mass contrast of the inorganic backbone. Upon assembly with proteins, multiple protein copies bind at the single polymer chain level resulting in structures reminiscent of compact spherical complexes or stiffened coils. The outcome depends on protein characteristics and cannot be deduced by commonly used characterization techniques, such as light scattering, thus revealing direct morphological insights crucial for understanding biological activity. Atomic force microscopy supports the morphology outcomes while advanced analytical techniques confirm protein-polymer binding. The chain visualization methodology provides tools for gaining insights into the processes of supramolecular assembly and mechanistic aspects of polymer-enabled vaccine delivery.

Polymer architecture and conformation – the spatial arrangement of the atomic groups in an individual chain – constitute the fundamental molecular basis, which essentially defines or significantly impacts physical and biological behavior of synthetic macromolecules[1–5]. Although the conformational analysis and direct visualization of naturally assembled rigid and semirigid macromolecular structures, such as proteins and polynucleotides, has been rapidly evolving, flexible synthetic polymers remain somewhat outside of this success story[6]. The selection of tools for studying, visualizing and controlling conformation of single-chain molecules of flexible synthetic polymers in solutions is still severely limited, mainly due to the propensity of these macromolecules to fold and aggregate under the conditions of the analysis[6]. Nevertheless, the structural and conformationally dynamic features of flexible chains, as they are exposed to various types of application related activities, can provide important clues to optimizing their performance and understanding their mechanism of action. This is especially important for physiologically active macromolecules and their interactions with living systems.

Poly[di(carboxylatophenoxy)phosphazene], PCPP is a synthetic ionic macromolecule, which stands out from conventional polyelectrolytes due to its potent immunoadjuvant activity, which has been demonstrated in numerous in vivo studies and in the clinical environment[7–9]. The accumulated physico-chemical, biophysical and in vivo data reveal that PCPP realizes its biological activity through spontaneous self-assembly with antigenic proteins in aqueous solutions[7]. However, the comprehensive structural characterization of PCPP in aqueous solutions and its supramolecular assemblies with proteins has not yet been carried out. It is expected that understanding the mechanism of supramolecular assembly and detailed characterization of the resulting structures remains one of the key prerequisites for the successful development and optimization of this vaccine delivery system. Furthermore, direct measurements of conformational changes from intermolecular interactions between proteins and polyelectrolytes should provide insights on design of materials to modulate biological performance of polyelectrolyte-based biomaterials.

Cryogenic Electron Microscopy (cryo-EM) and Atomic Force Microscopy (AFM) remain some of the most advanced and prevalent techniques for visualizing single biomacromolecules. Cryo-EM provides real-space microscopy images of biomolecules embedded in vitreous, glass-like ice shedding light on the behavior of macromolecules in their native environment[10–13]. The technique is rapidly becoming an attractive method in the field of structural biology with molecular structures as small as the 52 kDa streptavidin and the 40 kDa ribonucleic acid (RNA) are within the practical limits of characterization[10]. More recently, cryo-EM has also

[1]Institute for Bioscience and Biotechnology Research, University of Maryland, Rockville, MD 20850, USA. [2]Materials Science and Engineering Division, Material Measurement Laboratory, National Institute of Standards and Technology‡, 100 Bureau Drive, Gaithersburg, MD 20899, USA. e-mail: aandrianov@umd.edu

become a game-changing tool not only in protein structure determination, but also in protein assemblies, protein ligand–receptor interactions, and, now, assemblies of synthetic peptides[14,15]. However, being developed as a predominantly biological technique, the use of cryo-EM to study synthetic polymers and soft matter has been much more limited mainly due to insufficient electron-optical image contrast in polymers composed of lighter elements[16–18] and their inherent flexibility that prevents robust multi-particle averaging that is key to atomic resolution single particle reconstruction of protein molecules. Therefore, most of cryo-EM research on synthetic polymers has been focused not on visualization of individual chains of linear polymers, but on investigations of high mass contrast systems, such as their supramolecular assemblies, polymer-based fibers and micelles. Those structures of higher polymer hierarchy are typically represented by filaments formed by helical polypeptides[15,17], dendronized polymers[19–22], spherical[23] or cylindrical[24–26] polyelectrolyte brushes with dense side chains, various micellar assemblies[27–30], non-polymer based nanotubes of an amphiphilic cyanine dye[31], aggregates formed by polyelectrolyte complexes[32] or stacking of the conjugated polymer in organic solvents[33]. In contrast, AFM has been successfully employed for imaging single-chain linear synthetic polyelectrolytes, however this technique only allows visualization of macromolecules in their adsorbed state[34–37]. It can be expected that the complementary information provided by two methods, which exploit distinctly different experimental techniques, can offer invaluable insights into solution behavior of PCPP and its self-assembly with model protein systems. Alternate approaches, such as small-angle neutron scattering provide average chain conformation and rely on isotopic labeling in order to directly measure the form factor of a chain molecule, which is related by Fourier transform to the pair distribution function and by convolution to real-space density distribution[38]. Therefore, models must be applied to relate the reciprocal space to the real-space trial structure due to the classical phase problem in scattering[39].

Here we successfully visualized and compared images of individual chains of a linear synthetic polymer, PCPP, in aqueous solution in its vitrified and surface adsorbed states. Both cryo-EM and AFM methods demonstrated spontaneous association of PCPP with model antigenic proteins – bovine serum albumin (BSA) and hen egg lysozyme. Two distinct scenarios of complex formation were revealed. While self-assembly with BSA occurred without noticeable changes in polymer conformation, significant compaction of linear chains was observed for lysozyme. This was manifested in the formation of loops and re-crossed chains by cryo-EM and formation of spherical caps of adsorbed complexes by AFM. Given previously demonstrated in vivo immunopotentiating effect of PCPP with either of the studied proteins[40,41], the structural insights provided by cryo-EM and AFM can offer important clues in studying the mechanism of biological activity of this important macromolecular immunoadjuvant. Such measurements offer unique data needed to interpret measurements, such as dynamic light scattering and small-angle X-ray and neutron scattering in polyelectrolyte-protein complex solutions.

Results

Direct visualization of individual PCPP chains using cryo-EM and AFM methods

PCPP is a weak synthetic polyelectrolyte with the mass-average molar mass of 800,000 g mol^{-1}, which is fully soluble under neutral and basic conditions[42]. Its molecular structure includes two carboxylate moieties per repeat unit (Fig. 1a). Cryo-EM images of PCPP samples prepared in a vitrified state from solution in a phosphate buffer at pH 7.4 show clearly visible polymer chains (Fig. 1a, b and Supplementary Fig. 1). Their appearance can be described as random coils of various length with a majority exceeding 100 nm in size. Some loose loops can be noticed in the images, but no apparent re-crossing is visible. The density of macromolecular chains visible in cryo-EM images was dependent on the polymer concentration in the sample. Highly crowded fields observed at 2.5 mg mL^{-1} PCPP contrasted with images of isolated macromolecules, which were obtained at five-fold dilution (Supplementary Fig. 1a, b).

Investigation of PCPP chains by AFM was initially impeded by difficulties in adsorbing the anionic polyphosphazene macromolecule on the surface of freshly-cleaved mica. To obtain sufficient adhesion of PCPP to the inorganic surface, mica was modified with bovine serum albumin (BSA) (Supplementary Fig. 2). AFM images of PCPP adsorbed on such surfaces are shown in Supplementary Fig. 1d, e and in Supplementary Fig. 3a. Although, the dimensions of adsorbed PCPP chains appear to be somewhat larger than those detected in vitrified samples, PCPP coils visualized by both methods appear to be of similar shape. This may reflect that adsorption of PCPP is favored for higher molar mass with the smaller chains rinsed off during the sample preparation step.

Self-assembly of PCPP-BSA complexes as revealed by cryo-EM

To evaluate the potential effect of BSA on PCPP chains visualized by AFM, protein-polymer solutions in their vitrified form were also studied by cryo-

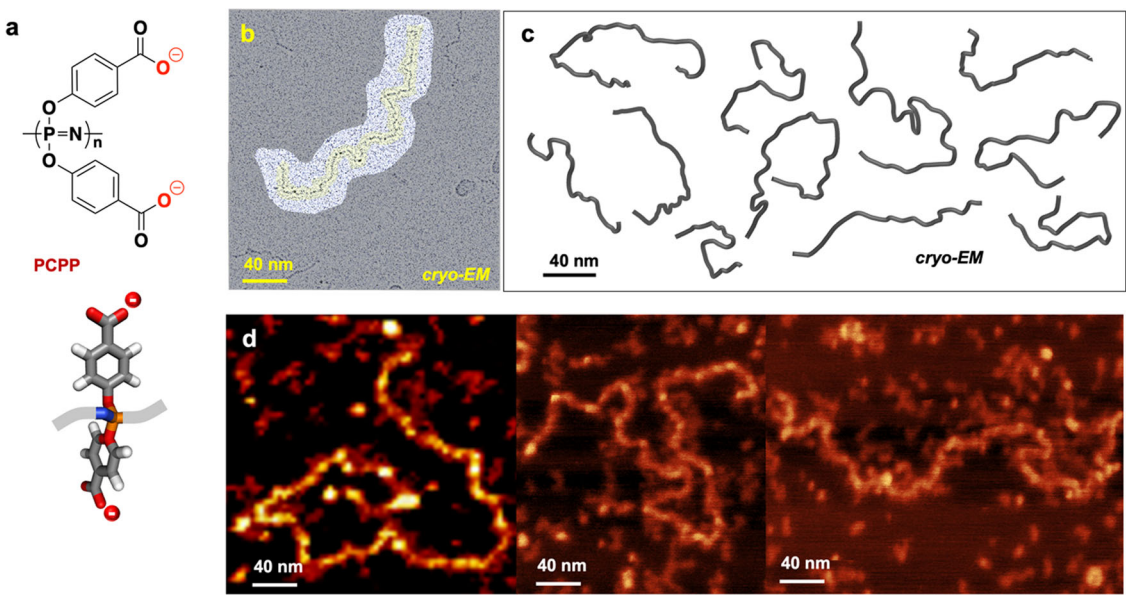

Fig. 1 | Visualization of individual PCPP chains. a Chemical structure of PCPP repeat unit. **b** Cryo-EM image of a single PCPP chain (defocus 2.12. μm) and (**c**) projections of representative polymer chain trajectories obtained from cryo-EM images shown in Supplementary Fig. 1. **d** AFM images of individual PCPP chains.

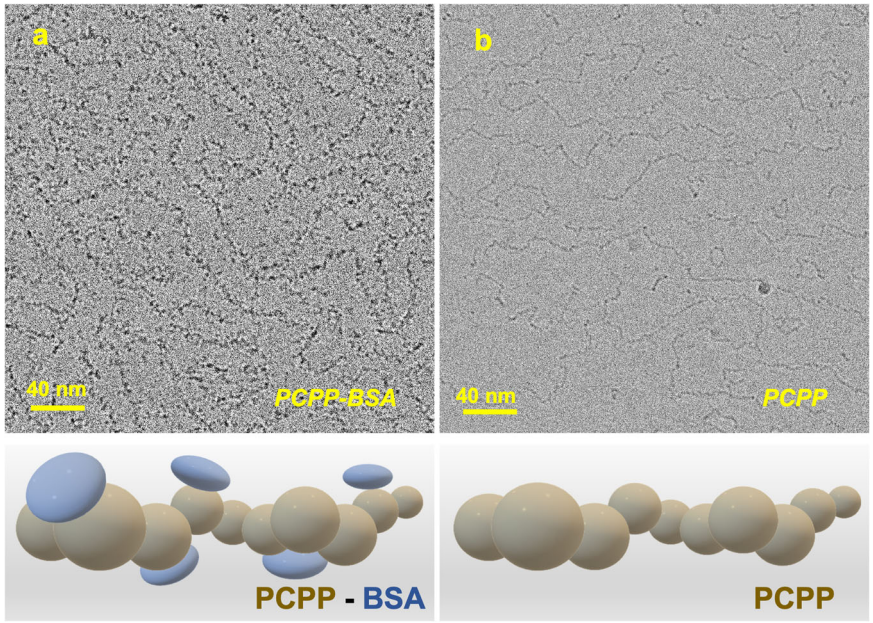

Fig. 2 | Contrasting of PCPP with BSA. Cryo-EM images of (**a**) PCPP-BSA (defocus 2.01 μm) and (**b**) PCPP (defocus 0.10 μm) (2.5 mg mL^{-1} PCPP, 0.25 mg mL^{-1} BSA, 50 mmol phosphate buffer, pH 7.4).

EM. BSA is a globular protein with molar mass of 66 kDa, which was characterized with small-angle neutron scattering as a prolate ellipsoid with $a = (7.0 \pm 0.2)$ nm and $b = (2.0 \pm 0.1)$ nm with the radius of gyration of 3.05 nm, where a and b are the semi-major and minor axes, respectively[43]. The image of PCPP-BSA mixture shows the assembly of small dots along the curved lines (Fig. 2a). These densely dotted lines resemble chains of free PCPP visualized under the same experimental conditions (Fig. 2b), but show a superior contrast. Essentially, the approach can be considered as 'decorating' of PCPP chains through the association of synthetic macromolecule with BSA. These results are in line with previous reports on noncovalent association of BSA and PCPP demonstrated by size exclusion chromatography and asymmetric flow field flow fractionation (AF4)[40,44]. The comparison of Fig. 2a, b suggests no significant 'disturbing' effect of BSA binding on the conformation of the polymer. These results, along with DLS studies on the effect of BSA on the dimensions of PCPP (Supplementary Fig. 3b), indicate that any potential influence of BSA on the conformation of PCPP chains shown in AFM generated images (Fig. 1d and Supplementary Fig. 3a) is minor.

Interactions of PCPP with positively charged protein – lysozyme

Hen egg lysozyme, a protein with a large positively charged surface area (Fig. 3a), forms complexes with PCPP at neutral pH[45,46]. Although such interactions typically result in a severe aggregation and phase separation[45], PCPP-lysozyme mixtures prepared at 1:7 polymer-to-protein mole ratio are essentially clear solutions with no aggregates detected by dynamic light scattering (DLS)(Supplementary Fig. 4). Fluorescence quenching data and size exclusion chromatography analysis provide clear indication of binding in the system (Fig. 3b, c), while zeta potential distribution profiles suggest that this is an electrostatically driven process (Fig. 3d). Nevertheless, the above-mentioned data, along with the isothermal titration calorimetry results indicating the dissociation constant of the complex below the micromolar range (Supplementary Fig. 5 and Supplementary Table 1), do not yet constitute a proof of the single-chain complex formation as the coexistence of free PCPP chains and larger aggregates still cannot be ruled out completely. To that end, the analysis of complexes using cryo-EM and AFM methods could provide critical information on the mechanism of complexation in this system, which is important for further understanding of the mechanism of immunoadjuvant activity of PCPP.

Representative cryo-EM images of vitrified samples of PCPP-lysozyme mixtures (1:7 mole ratio) and their chain trajectory are shown in Fig. 4a, b. The absolute majority of coils visible in the field are compact coils with dimensions significantly smaller than for free PCPP chains described above. The conformations show extensive looping and apparent re-crossing of chains. The size distribution obtained by encircling the images of individual coils (pervaded volume), (as shown in Supplementary Fig. 6) indicate that the majority of them can be characterized with diameters in the range of 20 nm to 40 nm (Fig. 4c). The size distribution obtained from cryo-EM measurements was compared with the results of DLS studies, in which the volume distribution was crudely assessed using Mie theory assuming spherical shape and homogeneity of complexes[47] (Fig. 4c). The comparison of results shows close similarity between distribution profiles, although DLS assessment revealed that the majority of complexes were in 10 nm to 30 nm diameter range.

AFM visualization of PCPP-lysozyme complexes was initially attempted using BSA-mediated adsorption on mica surface – the technique described above for free PCPP chains. Although some AFM images of complexes were collected (Supplementary Fig. 7), the best adsorption and image resolution was obtained by using mica surface pretreated with branched polyethyleneimine (bPEI) (Fig. 5a). In either case, images showed spherical caps with an average diameter of around 40 nm and 14 nm average height (Fig. 5b–d) with no individual chains detectable under conditions of the experiment. Although, AFM data provide somewhat more limited information compared to cryo-EM images, the results show a compaction of PCPP chains upon addition of lysozyme. The dimensions of the complexes as visualized by cryo-EM and AFM are comparable, especially if the anisotropy of the spherical cap (larger pervaded diameter) is attributed to the effect of surface adsorption in the sample preparation process. It should also be noted that similarly to protein molecules, PCPP could partially adsorb at the water-air interface[48–50] resulting in some increase of its apparent size in cryo-EM images. The effect might also be a result of drying out in atmospheric AFM as dehydration might lead to shrinkage of the structure.

Chain statistics

To quantify the flexibility of PCPP the imaged polymeric chains were traced to provide backbone contours for analysis of conformation. The tracing and conformational analysis was performed according to the SmarTrace algorithm[51]. Here the traced chains were randomly segmented to non-overlapped fragments of various contour length. Then for all of the segments squared end-to-end distance $\langle R^2(s) \rangle$ and the tangent vector correlation $\langle \cos\theta(s) \rangle$ length-dependent trends were compared with the predictions of

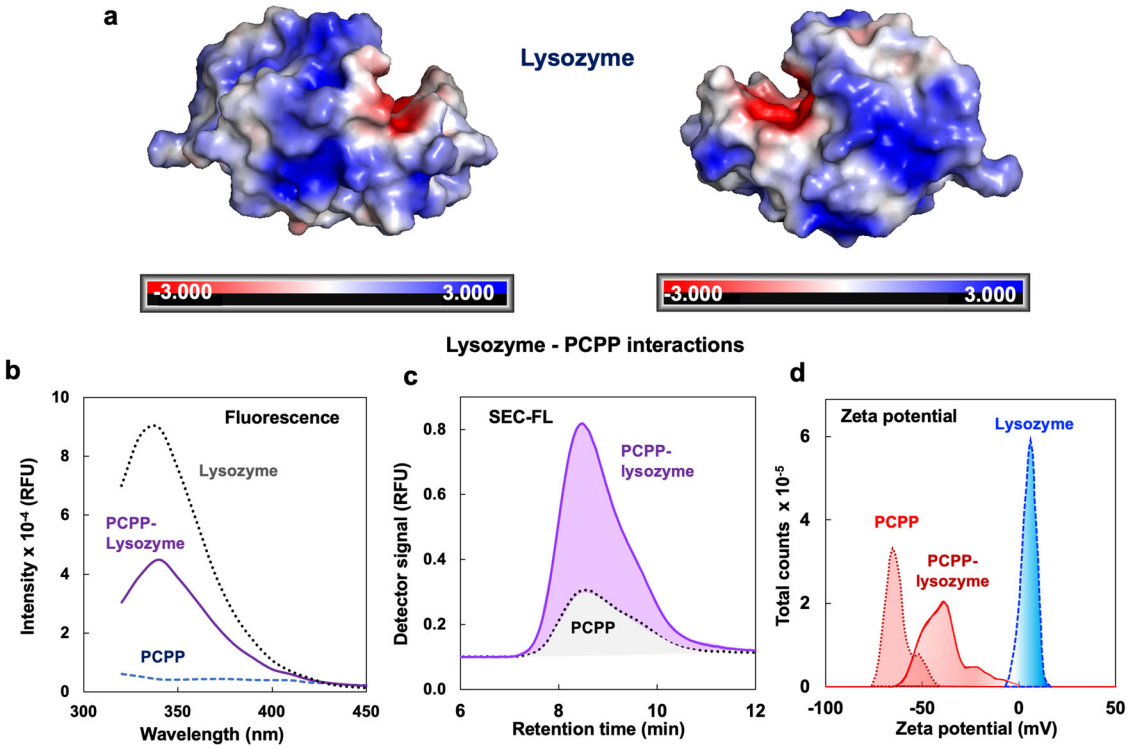

Fig. 3 | Interactions of PCPP with lysozyme. a Schematic presentations of electrostatic potential surfaces of hen egg lysozyme[64] (images generated using PyMOL 2.5.5 (Schrödinger Inc., New York, NY); **b** Fluorescence of lysozyme – dotted line, PCPP-lysozyme complex (1:7 mole mole^{-1}) – solid line and PCPP – dashed line (0.5 mg mL^{-1} PCPP, 0.06 mg mL^{-1} lysozyme, 50 mM phosphate buffer, pH 7.4, excitation wavelength: 280 nm); **c** size-exclusion chromatography profiles of PCPP-lysozyme – solid line and PCPP – dotted line (0.5 mg mL^{-1} PCPP, 0.06 mg mL^{-1} lysozyme, excitation/emission wavelengths: 280 nm/340 nm; 50 mM phosphate buffer, pH 7.4) (**d**) zeta-potential distribution profiles for PCPP – dashed line, lysozyme – dotted line and their mixture -solid line (0.5 mg mL^{-1} PCPP, 1 mg mL^{-1} lysozyme, complex: 0.5 mg mL^{-1} PCPP and 0.06 mg mL^{-1} lysozyme, 50 mM phosphate buffer, pH 7.4).

the worm-like chain (WLC) model for polymers (Supplementary Figs. 8–10). The persistence lengths for PCPP and PCPP/BSA are presented in Table 1.

Discussion

The evolving interest in PCPP and its structural analogs is primarily dictated by the potent immunoadjuvant effect demonstrated by this biodegradable macromolecule in multiple animal models and in clinical trials[7–9]. Immunoadjuvants are important components of contemporary vaccines, which enhance, prolong and modulate antigen-specific immune responses[52–54]. Although, the exact mechanisms of action still remain under discussion, the antigen delivery capabilities constitute some of the key features for many representatives of the class[55]. In particular, dispersed systems, such as aluminium hydroxide or phosphate (Alum or Alhydrogel), nanoemulsions, liposomes, polymer nanoparticulate are known to be capable of effective presentation of the antigen. Their dimensions and well-defined surface, on which the antigen is displayed, provide for virus-mimicking characteristics and largely enabling uptake by immunocompetent cells[55]. PCPP – a linear flexible macromolecule appears to lack those essential features, but nevertheless outperformed many of particulate adjuvants in vivo. Visualization of macromolecular architecture and conformation of PCPP, as well as their complexes with proteins in solutions constitute important prerequisites for understanding the mechanism of activity of this class of adjuvants.

Cryo-EM of conventional synthetic polymers, except of some highly branched structures and aggregates, has not been sufficiently advanced due to low mass contrast exhibited by most conventional macromolecules with carbon-carbon backbones. To that end, PCPP offered some interesting possibilities since it displays some structural similarities to DNA, which shows high mass contrast in cryo-EM studies due to its phosphorus containing backbone and electron-dense base pairs[21]. In fact, the phosphorus-nitrogen backbone of PCPP along with two aromatic side groups per repeat unit, enabled direct visualization of its macromolecular coils in samples prepared by vitrification of solutions at near physiological pH. To the best of our knowledge, this is the first report on a direct visualization of single chains of a linear synthetic polymer by cryo-EM. The observed images of individual chains were consistent with those obtained by AFM studies using surface adsorbed PCPP.

Further study on interactions of PCPP with BSA and lysozyme provides a direct proof of polymer association with proteins in aqueous solution. Moreover, in either case, the formation of complexes on the basis of a single polymer chain was observed with the absence of larger multi-chain aggregates. The latter were interpreted from previous studies by DLS and AF4, which are ensemble methods[45]. The sample processing for cryoEM imaging, such as blotting and vitrification, may remove such large aggregates, although it cannot be ruled out that simply a much larger statistics are needed in order to observe small populations of larger objects within the field of view at the studied stichometry of mixing. Furthermore, both ultrathin carbon support film (cryo-EM) and the BSA treated mica (AFM) may interact with PCPP and its complexes, therefore potentially causing some disturbing effect on their conformational states. However, multivalent cation-mediated adsorption of negatively charged macromolecules to mica is known to be driven by strong ionic interactions[56] and PCPP chains were retained on the surface even after rinsing (AFM studies). In contrast, the adsorption of polyacid on carbon was reported to be maximized only under acidic conditions, at which the polymer was weakly charged and coiled, and was greatly suppressed at neutral pH[57] – the conditions used in our cryoEM study.

It has to be noted that both proteins selected for the present study were successfully adjuvanted by PCPP in immunogenicity studies in vivo[40,41]. Therefore, the results provide important information relevant to the ongoing discussion on the mechanism of action of polyphosphazene adjuvants. The study revealed two distinct scenarios of the way PCPP

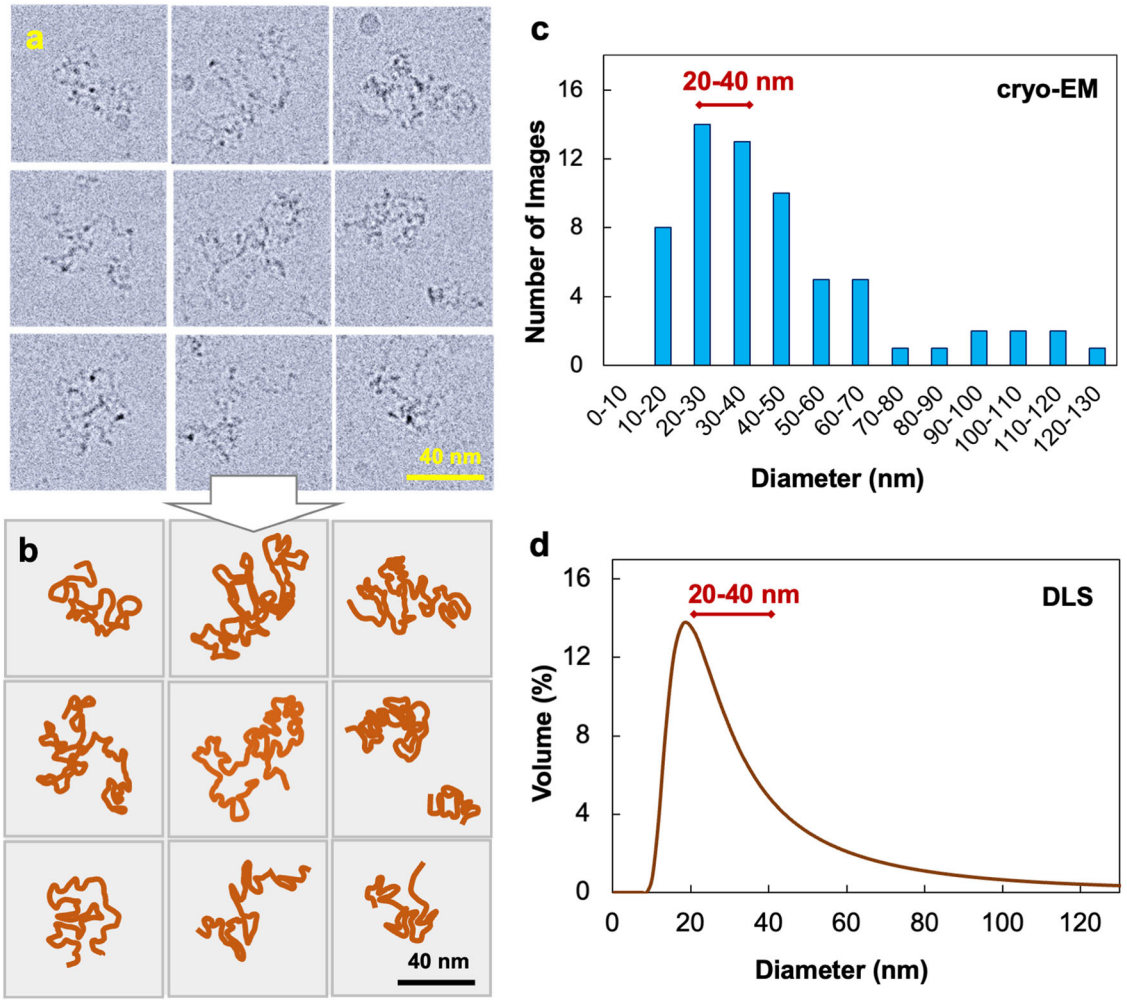

Fig. 4 | Visualization and characterization of PCPP complexes with lysozyme. **a**, **b** Cryo-EM images of PCPP-lysozyme complexes (1:7 mole ratio, 0.5 mg mL^{-1} PCPP and 0.06 mg mL^{-1} lysozyme, defoci: 0.10-2.50 µm) and projections of their chain trajectories. **c**, **d** Complex size distribution as determined by measuring pervaded diameters of coils in cryo-EM images and DLS.

spontaneously self-assembles with proteins in aqueous solution. BSA, a protein with an overall net-negative charge at physiological pH, associates with PCPP without introducing significant conformation changes in the polymer (Fig. 2). In contrast, interactions with lysozyme, which has a net-positive charge at neutral pH, are sufficiently strong to cause compaction of PCPP chains, which is demonstrated by both cryo-EM and AFM visualization (Figs. 4 and 5). Regardless of the resulting complex conformation, PCPP maintains its ability to enhance immunogenicity of either of these proteins[40,41]. Direct measurements will enable informed interrelationships on polyelectrolyte-protein binding mechanisms driven by electrostatic interactions or hydrophobicity and solvent quality arguments that may occur as in this work at the single chain level versus macrophase separation[58,59].

In silico visualization of interactions between PCPP and antigens would be an important future development. However, quantitative atomistic molecular dynamics simulations with validated force fields for PCPP are not available at the present time. Such simulations to study binding between protein and PCPP with explicit water would provide mechanistic insight into the current observations, especially with respect to the roles of electrostatic and Vander Waals or hydrophobic group influences on the binding. However, simulating the high molecular weights would be resource intensive, if not prohibitive. Therefore, in silico studies that consider the binding within a few persistence lengths would inform upon the local energetics, but lack the large-scale conformational changes. Such approaches are along the lines of the extensive research in structural biology where transient protein-protein interactions[60] and subsequently docking models[61] score the complexation. A development of tools along these lines that engage synthetic polymer and structural biology would be welcome.

Conclusions

The determination of vaccine particle structure represents a modern characterization challenge and world-wide interest. Advances in cryo-EM have enabled characterization of biomacromolecules in the vitrified state due to sufficient mass contrast between the compact protein globule or nucleic acid filaments and surrounding water. Synthetic polymers – flexible linear chains composed of lighter elements typically do not provide for sufficient electron-optical image contrast and have been visualized in their higher hierarchy states, such as supramolecular assemblies or filaments. Here, it was demonstrated that the phosphorus and nitrogen containing linear backbone, intrinsic to polyorganophosphazenes, enables substantial electron microscopy contrast to directly observe individual chains. The spontaneous self-assembly with antigenic proteins in the form of single-chain complexes was observed for the first time under conditions of 1:7 stoichiometry of mixing. The contrasting structures of PCPP complexes with BSA (net-negative) and lysozyme (net-positive) charge offer a more detailed view of the mechanism of self-assembly and the role of protein characteristics, such as their amphoteric character and charge heterogeneity. The stiffening of PCPP upon BSA binding, as revealed by the persistence length estimates,

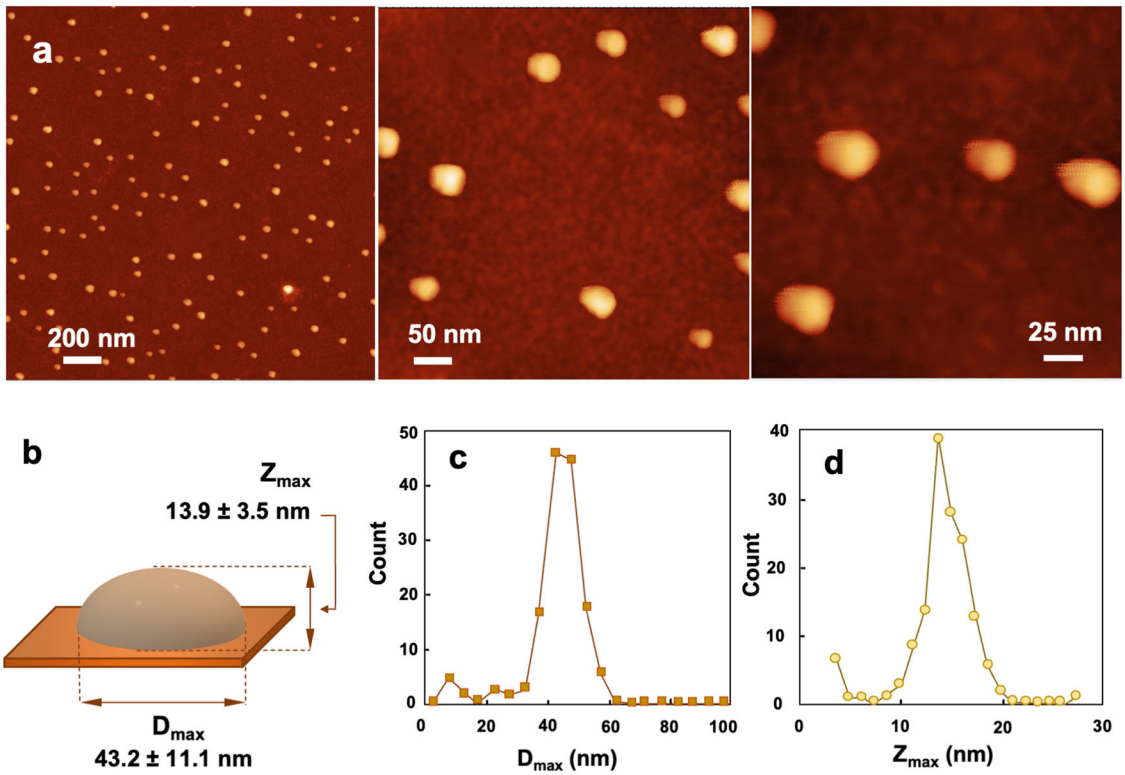

Fig. 5 | Visualization and characterization of PCPP using AFM. a AFM images at various magnifications. **b** Schematic presentation of adsorbed complex with average dimensions. **c**, **d** Diameter (solid-colored squares) and (open circles) height distribution of complexes (AFM images are taken from bPEI-treated mica substrates).

suggests a new mechanism that requires computer simulation modeling on how an already highly charged polyelectrolyte further stiffens. This contrasts with PCPP binding with lysozyme, which leads to some compactization of objects, reminiscent of condensation. In either case, the single chain complexes maintain immunoadjuvant potency due to the flexible and conformational dynamics that allow access to the antigenic protein. In general, the use of polyphosphazene macromolecules, which are well-known for their unprecedented structural diversity, can provide indispensable methodologies for direct visualization of polymer-based supramolecular self-assemblies and polymer-enabled drug delivery systems.

Methods

Certain equipment, instruments or materials are identified in this paper in order to adequately specify the experimental details. Such identification does not imply recommendation by the National Institute of Standards and Technology, nor does it imply the materials are necessarily the best available for the purpose. The symbols M and mM used to represent mol L^{-1} and mmol L^{-1}, respectively, and are not in SI units, but used to adhere to the conventions of the Journal.

Materials

Lysozyme from chicken egg white, BioUltra, lyophilized powder, ≥98% and bovine serum albumin, lyophilized powder, ≥96% (Sigma-Aldrich, Saint Louis, MO) were used as received. High molecular weight poly[di(carboxylatophenoxy)phosphazene], PCPP (800,000 g mol^{-1}) was synthesized as described previously[42,62].

Table 1 | Persistence lengths values (l_p) of PCPP obtained on the basis of AFM and cryo-EM measurements (the uncertainty (±) in the persistence length is given by standard deviation from the average value)

Polymer	l_p (nm)
PCPP-BSA (AFM)	17.8 ± 0.5
PCPP-BSA (Cryo-EM)	14.8 ± 0.3
PCPP (Cryo-EM)	7.7 ± 0.7

Cryogenic electron microscopy

A sample droplet of 3.0 μL was deposited on holey carbon film TEM grids (Q3100CR1.3-2 nm, Electron Microscopy Sciences, Hatfield, PA), which were plasma-treated beforehand using glow discharge PELCO EasiGlow (Ted Pella Inc., Redding, CA) for 15 s at 10 mA. The atmosphere for glow discharging was a residual air. The grids were then blotted twice for 2 s, each time at 12 °C and 100% humidity on the Vitrobot (Vitrobot Mark IV, FEI, Hillsboro, OR), leaving a thin layer stretched over the grid holes and vitrified in liquid ethane. The temperature was monitored and kept constant in the chamber during all the sample preparation steps. The samples then were transferred to 200 kV Talos Arctica (FEI, Hillsboro, OR) equipped with FEI Falcon3EC direct electron detector. Imaging was performed at temperature about 90 K at an acceleration voltage of 200 kV. The data were collected using EPU software (version 2.9.0) in a counting mode, the pixel size is 0.983 Å, the total electron dose is 48 e $Å^{-2}$. The total of 90 images of PCPP, 73 images of PCPP-BSA system and 95 images of PCPP-lysozyme system were collected using automated acquisition. The number of frames was 37 for PCPP, 45 for PCPP-BSA system and 30 for PCPP-lysozyme system. Patch motion correction and CTF correction were done in CryoSPARC 4.2.1 (Structural Biotechnology Inc., Toronto, Canada). The data collection statistics is shown in Supplementary Table 2. ImageJ software[63] was later used to tune the contrast and brightness of the acquired images. Some persistent background patterns are due to gain reference inconsistencies, but the results are not affected since no structural reconstructions are performed.

Atomic force microscopy

AFM studies were performed using a Bruker Dimension Icon AFM instrument (Bruker, Billerica, MA) in the ScanAsyst mode. The cantilever used for measurements was a ScanAsyst Air probe (Bruker, Billerica, MA) with resonant frequency 70 kHz, spring constant 0.4 N m^{-1}, and with a

nominal tip radius of 2.0 nm. The PCPP samples were deposited by dip coating from BSA/PCPP solution (BSA 0.25 mg mL^{-1}, PCPP 0.05 mg mL^{-1}) on freshly cleaved muscovite mica V1 (71856-01, Electron Microscopy Sciences, Hatfield, PA) for 5 min deposition time followed by rinsing and drying in nitrogen flow. The PCPP-lysozyme complexes were deposited by dip coating from (lysozyme 0.006 mg mL^{-1}, PCPP 0.05 mg mL^{-1}) solution on silicon wafers (⟨111⟩, 0.5 mm, Institute of Electronic Materials Technology, Poland) primed with bPEI for 5 min time followed by drying in nitrogen flow.

Dynamic light scattering and Zeta potential

DLS and Zeta potential measurements were performed using a Malvern Zetasizer Nano ZS (Malvern Instruments Ltd., Worcestershire, UK) using a 532 nm laser with a back-scattering detector an angle of 173° with data recorded and processed in Malvern Zetasizer Software 7.10. Polymer and protein were filtered through poly(vinylidene fluoride) (PVDF) Millex syringe filters (EMD Millipore, Billerica, MA) with a pore size of 0.22 μm prior to measurements. DLS measurements were performed at 25 °C using BRAND (BrandTech Scientific, Inc., Essex, CT) disposable ultra-micro cuvettes with plastic caps for polymer and complex formulations containing 0.5 mg mL^{-1} PCPP and a protein concentration of 0.5 mg mL^{-1} in 50 mM phosphate buffer, pH 7.4. Each measurement was averaged from 12 scans. Zeta potential measurements were performed at 25 °C using Malvern DTS1070 cuvettes (Malvern Instruments Ltd., Worcestershire, UK) for the same concentrations with the accumulation and averaging of 100 scans.

Isothermal titration calorimetry

ITC experiments were performed using a Nano ITC SV instrument (TA Instruments, Waters, New Castle, DE, USA) at 25 °C. In a typical experiment, 900 μL of PCPP solution was placed into isothermal chamber and was titrated by 10 μL aliquots of lysozyme from a 250 μL syringe rotating at 36.7 rad s with a 300 s delay between each injection. Each injection generated a heat release curve (microjoules per second versus seconds), which later was processed using NanoAnalyze software, version 3.12.5 (TA Instruments, Waters, New Castle, DE, USA) to yield the heat associated with each injection. Data analysis was performed with the above software and a single set of identical sites (SSIS) binding model was used to calculate thermodynamic parameters: binding constant (K_d), reaction stoichiometry (n), enthalpy (ΔH), and entropy (ΔS).

Fluorescence

Fluorescence measurements were performed using a BioTek SyNergy neo2 multimode reader (BioTek Instruments, Inc., Winooski, VT). Emission spectra were recorded at a fixed excitation wavelength of 280 nm.

Size-exclusion chromatography

SEC analysis of polymer and polymer/protein complex were conducted using an Agilent 1260 Infinity II Binary LC system (Agilent, Santa Clara, CA) equipped with a G7112B binary pump, G7167A Multisampler, G7116A multicolumn thermostat, G7117C diode array detector, G7121A fluorescence detector, and TSKgel GMPW size-exclusion column (Tosoh Bioscience, LLC, Japan); phosphate buffer (PBS) with 10 % acetonitrile volume fraction used as a mobile phase (0.75 mL min^{-1} flow rate, injection volume 50 μL).

Data availability

All relevant data are available from the corresponding author upon a reasonable request.

Received: 26 October 2023; Accepted: 7 March 2024;
Published online: 14 March 2024

References

1. Wang, Z.-G. 50th anniversary perspective: polymer conformation—a pedagogical review. *Macromolecules* **50**, 9073–9114 (2017).
2. Altintas, O. & Barner-Kowollik, C. Single-chain folding of synthetic polymers: a critical update. *Macromol. Rapid Commun.* **37**, 29–46 (2016).
3. Wang, S. & Urban, M. W. Self-healing polymers. *Nat. Rev. Mater.* **5**, 562–583 (2020).
4. Winkler, R. G., Elgeti, J. & Gompper, G. Active polymers — emergent conformational and dynamical properties: a brief review. *J. Phys. Soc. Jpn* **86**, 101014 (2017).
5. Vacha, M. & Habuchi, S. Conformation and physics of polymer chains: a single-molecule perspective. *NPG Asia Mater.* **2**, 134–142 (2010).
6. Knudsen, J. B. et al. Routing of individual polymers in designed patterns. *Nat. Nanotech* **10**, 892–898 (2015).
7. Andrianov, A. K. & Langer, R. Polyphosphazene immunoadjuvants: Historical perspective and recent advances. *J. Controlled Release* **329**, 299–315 (2021).
8. Magiri, R., Mutwiri, G. & Wilson, H. L. Recent advances in experimental polyphosphazene adjuvants and their mechanisms of action. *Cell Tissue Res* **374**, 465–471 (2018).
9. Chand D. J., Magiri R. B., Wilson H. L. & Mutwiri G. K. Polyphosphazenes as adjuvants for animal vaccines and other medical applications. *Front. Bioeng. Biotechnol.* **9**, 625482 (2021).
10. Weissenberger, G., Henderikx, R. J. M. & Peters, P. J. Understanding the invisible hands of sample preparation for cryo-EM. *Nat. Methods* **18**, 463–471 (2021).
11. Yip, K. M., Fischer, N., Paknia, E., Chari, A. & Stark, H. Atomic-resolution protein structure determination by cryo-EM. *Nature* **587**, 157–161 (2020).
12. Cheng, Y. Single-particle cryo-EM - How did it get here and where will it go. *Science* **361**, 876–880 (2018).
13. Gopal, A., Zhou, Z. H., Knobler, C. M. & Gelbart, W. M. Visualizing large RNA molecules in solution. *RNA* **18**, 284–299 (2012).
14. Tirrell, M. Polymorphism in peptide self-assembly visualized. *Proc. Natl Acad. Sci. USA* **119**, e2123197119 (2022).
15. Pieri, L. et al. Atomic structure of Lanreotide nanotubes revealed by cryo-EM. *Proc. Natl Acad. Sci. USA* **119**, e2120346119 (2022).
16. Lyu, Z., Yao, L., Chen, W., Kalutantirige, F. C. & Chen, Q. Electron microscopy studies of soft nanomaterials. *Chem. Rev.* **123**, 4051–4145 (2023).
17. Wang, F., Gnewou, O., Solemanifar, A., Conticello, V. P. & Egelman, E. H. Cryo-EM of Helical Polymers. *Chem. Rev.* **122**, 14055–14065 (2022).
18. Mai, D. J. & Schroeder, C. M. 100th anniversary of macromolecular science viewpoint: single-molecule studies of synthetic polymers. *ACS Macro Lett.* **9**, 1332–1341 (2020).
19. Jackson, C. L. et al. Visualization of Dendrimer Molecules by Transmission Electron Microscopy (TEM): Staining Methods and Cryo-TEM of Vitrified Solutions. *Macromolecules* **31**, 6259–6265 (1998).
20. Schlüter, A. D. et al. Dendronized polymers: molecular objects between conventional linear polymers and colloidal particles. *ACS Macro Lett.* **3**, 991–998 (2014).
21. Messmer, D. et al. 3D conformations of thick synthetic polymer chains observed by cryogenic electron microscopy. *ACS Nano* **13**, 3466–3473 (2019).
22. Berlepsch, H. et al. Controlled self-assembly of stomatosomes by use of single-component fluorinated dendritic amphiphiles. *Soft Matter* **14**, 5256–5269 (2018).
23. Wittemann, A., Drechsler, M., Talmon, Y. & Ballauff, M. High elongation of polyelectrolyte chains in the osmotic limit of spherical polyelectrolyte brushes: a study by cryogenic transmission electron microscopy. *J. Am. Chem. Soc.* **127**, 9688–9689 (2005).
24. Xu, Y. et al. Manipulating cylindrical polyelectrolyte brushes on the nanoscale by counterions: collapse transition to helical structures. *Soft Matter* **5**, 379–384 (2009).

25. Xu, Y. et al. pH and salt responsive poly(N,N-dimethylaminoethyl methacrylate) cylindrical brushes and their quaternized derivatives. *Polymer* **49**, 3957–3964 (2008).
26. Raguzin, I., Stoychev, G., Stamm, M. & Ionov, L. Single molecule investigation of complexes of oppositely charged bottle brushes. *Soft Matter* **9**, 359–364 (2013).
27. Parry, A. L., Bomans, P. H. H., Holder, S. J., Sommerdijk, N. A. J. M. & Biagini, S. C. G. Cryo electron tomography reveals confined complex morphologies of tripeptide-containing amphiphilic double-comb diblock copolymers. *Angew. Chem., Int Ed.* **47**, 8859–8862 (2008).
28. Wu, H., Ting, J. M. & Tirrell, M. V. Mechanism of dissociation kinetics in polyelectrolyte complex micelles. *Macromolecules* **53**, 102–111 (2020).
29. Lueckheide, M., Vieregg, J. R., Bologna, A. J., Leon, L. & Tirrell, M. V. Structure–property relationships of oligonucleotide polyelectrolyte complex micelles. *Nano Lett.* **18**, 7111–7117 (2018).
30. Marras, A. E., Vieregg, J. R., Ting, J. M., Rubien, J. D. & Tirrell, M. V. Polyelectrolyte complexation of oligonucleotides by charged hydrophobic—neutral hydrophilic block copolymers. *Polymers* **11**, 83 (2019).
31. Deshmukh A., et al. Near-Atomic Resolution Structure of J-aggregated Helical Light Harvesting Nanotubes. *ChemRxiv*, 2022. https://doi.org/10.26434/chemrxiv-2022-5m8sx.
32. Meng, S., Ting, J. M., Wu, H. & Tirrell, M. V. Solid-to-liquid phase transition in polyelectrolyte complexes. *Macromolecules* **53**, 7944–7953 (2020).
33. Wirix, M. J. M., Bomans, P. H. H., Friedrich, H., Sommerdijk, N. A. J. M. & de With, G. Three-dimensional structure of P3HT assemblies in organic solvents revealed by Cryo-TEM. *Nano Lett.* **14**, 2033–2038 (2014).
34. Kozhuharov, S., Radiom, M., Maroni, P. & Borkovec, M. Persistence Length of Poly(vinyl amine): quantitative image analysis versus single molecule force response. *Macromolecules* **51**, 3632–3639 (2018).
35. Kozhuharov, S., Maroni, P. & Borkovec, M. In situ imaging of single polyelectrolyte chains with the atomic force microscope. *Chimia* **73**, 17–20 (2019).
36. Minko, S. & Roiter, Y. AFM single molecule studies of adsorbed polyelectrolytes. *Curr. Opin. Colloid Interface Sci.* **10**, 9–15 (2005).
37. Roiter, Y. & Minko, S. AFM Single Molecule Experiments at the Solid−Liquid Interface: In Situ Conformation of Adsorbed Flexible Polyelectrolyte Chains. *J. Am. Chem. Soc.* **127**, 15688–15689 (2005).
38. Higgins J. S., Benoit H. C. Polymers and Neutron Scattering 1–23 (Oxford University Press, 1994).
39. Wei Y. & Hore M. J. A. Characterizing polymer structure with small-angle neutron scattering: A Tutorial. *J. Appl. Phys.* **129**, 171101 (2021).
40. Andrianov, A. K., Marin, A. & Roberts, B. E. Polyphosphazene polyelectrolytes: A link between the formation of noncovalent complexes with antigenic proteins and immunostimulating activity. *Biomacromolecules* **6**, 1375–1379 (2005).
41. Kovacs-Nolan J, Mapletoft JW, Latimer L, Babiuk LA, van Drunen Littel-van den Hurk, S. CpG oligonucleotide, host defense peptide and polyphosphazene act synergistically, inducing long-lasting, balanced immune responses in cattle. *Vaccine* **27**, 2048–2054 (2009).
42. Andrianov, A. K., Svirkin, Y. Y. & LeGolvan, M. P. Synthesis and biologically relevant properties of polyphosphazene polyacids. *Biomacromolecules* **5**, 1999–2006 (2004).
43. Bendedouch, D. & Chen, S. H. Structure and interparticle interactions of bovine serum albumin in solution studied by small-angle neutron scattering. *J. Phys. Chem.* **87**, 1473–1477 (1983).
44. Andrianov, A. K., Marin, A. & Fuerst, T. R. Molecular-Level Interactions of Polyphosphazene Immunoadjuvants and Their Potential Role in Antigen Presentation and Cell Stimulation. *Biomacromolecules* **17**, 3732–3742 (2016).
45. Lueckheide, M. et al. Monitoring Protein Complexation with Polyphosphazene Polyelectrolyte Using Automated Dynamic Light Scattering Titration and Asymmetric Flow Field Flow Fractionation and Protein Recognition Immunoassay. *ACS Polym. Au* **3**, 354–364 (2023).
46. Marin, A., Taraban, M. B., Patel, V., Yu, Y. B. & Andrianov, A. K. Supramolecular protein-polyelectrolyte assembly at near physiological conditions - water proton NMR, ITC, and DLS Study. *Molecules* **27**, 7424 (2022).
47. Stetefeld, J., McKenna, S. A. & Patel, T. R. Dynamic light scattering: a practical guide and applications in biomedical sciences. *Biophys. Rev.* **8**, 409–427 (2016).
48. D'Imprima, E. et al. Protein denaturation at the air-water interface and how to prevent it. *eLife* **8**, e42747 (2019).
49. Glaeser, R. M. & Han, B.-G. Opinion: hazards faced by macromolecules when confined to thin aqueous films. *Biophy Rep.* **3**, 1–7 (2017).
50. Noble, A. J. et al. Reducing effects of particle adsorption to the air–water interface in cryo-EM. *Nat. Methods* **15**, 793–795 (2018).
51. Rezaei, N., Lyons, A. & Forde, N. R. Environmentally Controlled Curvature of Single Collagen Proteins. *Biophys. J.* **115**, 1457–1469 (2018).
52. Pulendran, B., S. Arunachalam, P. & O'Hagan, D. T. Emerging concepts in the science of vaccine adjuvants. *Nat. Rev. Drug Discov.* **20**, 454–475 (2021).
53. Del Giudice, G., Rappuoli, R. & Didierlaurent, A. M. Correlates of adjuvanticity: A review on adjuvants in licensed vaccines. *Semin. Immunol.* **39**, 14–21 (2018).
54. Reed, S. G., Orr, M. T. & Fox, C. B. Key roles of adjuvants in modern vaccines. *Nat. Med* **19**, 1597–1608 (2013).
55. Bo, Y. & Wang, H. Materials-based vaccines for infectious diseases. *WIREs Nanomed. Nanobiotechnol* **14**, e1824 (2022).
56. Pastré, D. et al. Anionic polyelectrolyte adsorption on mica mediated by multivalent cations: a solution to DNA imaging by atomic force microscopy under high ionic strengths. *Langmuir* **22**, 6651–6660 (2006).
57. Wiśniewska, M. et al. Nanostructure of Poly(Acrylic Acid) adsorption layer on the surface of activated carbon obtained from residue after supercritical extraction of hops. *Nanoscale Res Lett.* **12**, 2 (2017).
58. Obermeyer, A. C., Mills, C. E., Dong, X.-H., Flores, R. J. & Olsen, B. D. Complex coacervation of supercharged proteins with polyelectrolytes. *Soft Matter* **12**, 3570–3581 (2016).
59. Kim, S. et al. Effect of protein surface charge distribution on protein–polyelectrolyte complexation. *Biomacromolecules* **21**, 3026–3037 (2020).
60. Nooren, I. M. A. & Thornton, J. M. Structural characterisation and functional significance of transient protein–protein interactions. *J. Mol. Biol.* **325**, 991–1018 (2003).
61. Jandova, Z., Vargiu, A. V. & Bonvin, A. M. J. J. Native or Non-Native Protein–Protein Docking Models? Molecular Dynamics to the Rescue. *J. Chem. Theory Comput* **17**, 5944–5954 (2021).
62. Andrianov, A. K., Chen, J. & LeGolvan, M. P. Poly(dichlorophosphazene) as a precursor for biologically active polyphosphazenes: Synthesis, characterization, and stabilization. *Macromolecules* **37**, 414–420 (2004).
63. Schneider, C. A., Rasband, W. S. & Eliceiri, K. W. NIH Image to ImageJ: 25 years of image analysis. *Nat. Methods* **9**, 671–675 (2012).
64. Weiss, M. S., Palm, G. J. & Hilgenfeld, R. Crystallization, structure solution and refinement of hen egg-white lysozyme at pH 8.0 in the presence of MPD. *Acta Cryst.* **56**, 952–958 (2000).

Acknowledgements

This work was supported in part by the National Institutes of Health Grant 1R01AI168048-01 (A.K.A.) and by the University of Maryland Strategic Partnership: MPowering the State.

Author contributions

A.K.A. and V.M.P. conceived the research and oversaw the project. V.M.P., A.K.A. and R.H. designed AFM study. R.H. prepared samples and conducted AFM experiments. A.K.A., E.P. and R.H. designed cryo-EM study. R.H. prepared samples, performed biophysical characterization and conducted cryo-EM experiments with help from E.P. R.H. carried out conformation analysis of polymer chains and calculations of their size distribution. A.K.A. and V.M.P. provided project supervision and coordination. A.K.A. wrote the original draft of the manuscript with multiple inputs from V.M.P. All authors approved the submitted version.

Competing interests

The authors declare no competing interests.

Additional information

Supplementary information The online version contains supplementary material available at https://doi.org/10.1038/s43246-024-00476-6.

Correspondence and requests for materials should be addressed to Alexander K. Andrianov.

Peer review information *Communications Materials* thanks Farzad Hamdi and the other, anonymous, reviewer(s) for their contribution to the peer review of this work. Primary Handling Editors: Jet-Sing Lee.